

Electromigration-induced void drift and coalescence: Simulations and a dynamic scaling theory

Kevin M. Crosby and R. Mark Bradley

Department of Physics, Colorado State University, Fort Collins, Colorado 80523

Hervé Boularot

Analyt GmbH & Company KG, Klosterrunsstrasse 18, 79379 Müllheim, Germany

(Received 14 March 1997)

Electromigration-induced failure of conductors in integrated circuitry is precipitated by the formation, drift, and coalescence of voids within the conductor. The kinetics of a collection of such voids is studied here through the development of a dynamic scaling theory, as well as through Monte Carlo simulations. In our model, voids originate at a source, drift with speeds inversely proportional to their radii, and coalesce according to a capture cross section which accounts for the effects of current crowding around the voids in an approximate fashion. The presence of a source leads to a spatially inhomogeneous distribution function $n(\Omega, x, t)$ for voids of volume Ω drifting in the x direction. We show that $n(\Omega, x, t)$ obeys the scaling form $n(\Omega, x, t) = \Omega^{-5/3} f(\Omega e^{-\rho x}, \Omega t^{-3})$ where $\rho \cong 0.054$ and f is a scaling function. We also obtain scaling solutions for the void fraction $\phi(x, t)$ which agree well with the simulations. At a fixed time, ϕ grows monotonically with distance from the source, reaches a peak, and then decreases exponentially with distance. The position of the peak is shown to move with a velocity $v \propto 1/t$. [S0163-1829(97)08637-2]

I. INTRODUCTION

Under normal operating conditions, the metal lines or interconnects in a very-large-scale integrated (VLSI) circuit carry high current densities, and this leads to drift of the metal ions and to the eventual failure of the circuit. This ionic motion is known as electromigration (EM).¹⁻³ With the progressive miniaturization of circuit components, EM failure of aluminum interconnects remains one of the principal factors limiting the reliability of integrated circuits. EM can lead to the failure of an interconnect in relatively short times, reducing the circuit lifetime to an unacceptable level. It is therefore of great technological importance to understand and control electromigration failure in thin films.

Two opposing forces act on an ion in a current-carrying wire. The momentum transfer from the conduction electrons results in a wind force, while the ambient electric field results in a direct force on the ion. Both forces are proportional to the electric field \vec{E} and it is customary to write $\vec{F}_{\text{ion}} = Z^* e \vec{E}$. Here \vec{F}_{ion} is the total force acting on an ion in the bulk and $Z^* e$ is the effective charge of the ion. Z^* is positive if the direct force is dominant, and is negative if the wind force is the stronger of the two forces. The latter possibility is not academic: Z^* is negative for aluminum, and aluminum (alloyed with small amounts of copper and silicon) is universally used as the material for interconnects in modern VLSI technology. Ions at a metal surface also move in the presence of an electrical current. In general, the effective charge for surface electromigration, Z_s^* , differs from Z^* .

Unfortunately, this drift of matter is not homogeneous. At some points in the line, the divergence of the mass flux is positive and voids appear. The mass flux converges at other points and this can lead to the formation of hillocks at the surface of the conductor. Both of these types of defect can

lead to the failure of a VLSI circuit.^{4,5}

In practice, the damage caused by the formation of hillocks can be controlled by passivating the interconnect, i.e., by covering the exposed surface of the line with a protective layer of glass. On the other hand, passivating the line does not prevent the formation and growth of voids and so only postpones failure. Void-induced failure occurs in the following way: After a time, the vacancies in the line become supersaturated and small spherical voids nucleate within the aluminum film. EM causes the ions located on the surface of a void to move from the upstream part of the void to the downstream one. As a result, the voids drift in the direction of the ambient electric field. Ho's analysis of this drift shows that an isolated spherical void preserves its shape as it moves and that its speed is inversely proportional to its radius.⁶ Moreover, it has recently been demonstrated that isolated voids are stable against small perturbations of their shape.^{7,8} Since small voids drift more rapidly than large ones, voids collide and coalesce. Ultimately, at the end of the failure process, a void spans the line and interrupts the flow of electrical current. While there have been some preliminary experimental investigations of void statistics,⁹ there have been no conclusive studies demonstrating general relationships between conductor lifetime and void distribution statistics.

In the relatively wide metal interconnects used in early VLSI circuits, the interconnect width was several times greater than the mean grain size. In these wires, ionic transport proceeds mainly by grain boundary diffusion driven by electromigration.⁴ Typically, voids are formed at grain boundary triple points, and these grow in size until electrical failure is complete. Since 1971, a number of simulations of the failure of such polycrystalline metal lines have been performed.¹⁰⁻¹⁹ In each case, it was assumed that the voids are stationary.

The failure of metal lines whose width approaches the grain size is quite different, as first shown by Vaidya *et al.*²⁰

These workers fabricated a group of polycrystalline Al–0.5% Cu wires with a range of widths but a common length, thickness, and mean grain size. The wires were then subjected to EM lifetime testing with a fixed current density. Vaidya *et al.* found that as the linewidth is reduced, the lifetime at first decreases, but then begins to increase dramatically.

The increase in lifetime begins as the width of the wire approaches the mean grain size. Wires with widths comparable to the mean grain size are called bamboo lines. In contrast with thicker wires, in bamboo or near bamboo lines there is no continuous path of grain boundaries that runs the entire length of the wire. These lines have substantially increased lifetimes as a result. In the near future, most interconnects will likely be bamboo aluminum lines, and so understanding their failure is an important practical issue. In this paper, we consider *single-crystal* metal lines. An understanding of the failure of single-crystal metal lines is an important first step toward an understanding of the failure of bamboo lines.

Little theoretical work has been devoted to the failure of single-crystal metal films through void drift and coalescence. Wickham and Sethna introduced a lattice model for void nucleation, drift, and growth in a single-crystal metal thin film.²¹ Although this work represents an important first step, the model of Wickham and Sethna suffers from some serious deficiencies: For example, current crowding around voids is entirely neglected, and the large voids drift more rapidly than the smaller voids, contrary to Ho's theory.

Recently, two of the present authors introduced a mean field theory of the drift and coalescence of circular voids in a current-carrying thin film.²² Current crowding around the voids was explicitly accounted for, albeit in an approximate fashion. The mean field equations were numerically solved for the void size distribution. It was shown that the distribution obeys a scaling form at long times. This preliminary study has some limitations, however. In real current-carrying wires the voids are spherical, and only become cylindrical once they have grown to sufficient size. A more significant limitation of the mean field theory of Boularot and Bradley²² is the assumption of a spatially homogeneous distribution of voids. In a real current-carrying wire, as mass leaves the wire at the anode, small voids appear within the film. These voids drift toward the cathode, and as they do, they collide, coalesce, and grow in size. The resulting void size distribution has a nontrivial dependence on position.

In this paper, we develop a dynamic scaling theory for the size and spatial distribution of drifting and coalescing spherical voids in the bulk. By electing to study the problem in the bulk, we sidestep the added complication of a three-dimensional (3D) to 2D crossover as the volume of the voids increases. This crossover could be incorporated in later work; the present work is meant only to be a first step toward understanding the behavior of a collection of many voids. We show that the usual scaling ansatz fails for the case in which spatial variations are permitted, and that a marginal scaling hypothesis is necessary. Few studies of spatially dependent coagulation equations exist in the literature,^{23–25} and little is known about the scaling properties or even the existence of physical solutions. The theory developed here represents an extension of standard coagulation models and al-

lows us to derive asymptotic forms for the void size distributions which differ qualitatively from those obtained in the absence of spatial variations. We also present results of simulations of the drift and coalescence of voids in long wires. We show that the predictions of the dynamic scaling theory for the asymptotic properties of the void distributions are in good agreement with the simulations and we obtain scaling exponents which agree quite well with the theory.

Simulations of a somewhat similar coalescence process have been performed by Meakin.^{26,27} In his work, bubbles of size s drift with speeds $v(s) \propto s^{\eta}$. When two or more bubbles touch, they coalesce and the resulting bubble's volume is the sum of the constituent volumes. The case $\eta < 0$, of which EM is a special case, was studied in one dimension only. The two- and three-dimensional simulations were carried out on a lattice to facilitate simulations with a large density of bubbles. In contrast, in our simulations of void drift, it is presumed that the void fraction is everywhere small. The most important distinction between our work and Meakin's, however, is that Meakin's bubbles move ballistically, while in EM one void can be deflected by another.

This paper is organized as follows. In Sec. II, we present the mean field equation of motion governing the void kinetics and obtain the coalescence cross section for two-void interactions. In Secs. III and IV, scaling solutions are obtained for the equation of motion, as well as the steady state properties of the void size distribution. The algorithm for the EM simulations and the simulation results are presented in Sec. V. In Sec. VI, we summarize our results.

II. MEAN FIELD EQUATION OF MOTION

In accordance with Ho,⁶ we will assume, first, that the motion of an isolated spherical void is parallel to the electric field, and, second, that its speed v is inversely proportional to its radius. Thus, if Ω is the volume of the void, $v = v(\Omega) = k\Omega^{-1/3}$, where the constant of proportionality k depends on the film material, the temperature, and the current density. Since the smaller voids drift more rapidly than the larger ones, collisions between voids will occur. When two voids of volume Ω_1 and Ω_2 collide, they coalesce and deform rapidly (instantaneously in our model) to form a single spherical void of volume $\Omega_1 + \Omega_2$. In this way, the surface energy is minimized subject to the constraint that the void volume is conserved. The position of the new void of volume $\Omega_1 + \Omega_2$ is known because the center of mass is unchanged by the coalescence event.

Consider the collision of two isolated spherical voids of volume Ω_1 and Ω_2 , where $\Omega_2 < \Omega_1$. Far from the larger void, the electric field is essentially uniform. As a result, the motion of the smaller void is nearly rectilinear when the voids are far apart. The same is true of the motion of the larger void. The electrical current is crowded by the larger of the two voids, however. As a result, the smaller void is deflected away from its initially linear trajectory as it approaches the larger void. The capture cross section $\sigma(\Omega_2, \Omega_1)$ is therefore smaller than it would be if the motion of the voids were simply rectilinear (the case of ballistic coalescence).

To account for this effect, we consider two isolated voids in an ambient electric field. As the probability of collisions

between voids of comparable size is small, most coalescence events will involve voids with quite disparate volumes. With this in mind, we neglect the deflection of the larger void away from its linear trajectory. It is convenient to introduce a moving coordinate system with origin coincident with the larger void's center of mass. We orient the axes so that the electric field far from the voids lies in the x direction. In the absence of the smaller void, the electrical current far from the large void is uniform and parallel to the ambient electric field. The electrical potential $\Phi_e(r, \theta)$ outside the large void is

$$\Phi_e(r, \theta) = -E_0 r \left[1 + \frac{1}{2} \left(\frac{R}{r} \right)^3 \right] \cos \theta. \quad (1)$$

Here, E_0 is the strength of the electric field far from the void, R is the radius of the larger void, and r and θ are polar coordinates. We assume that the smaller void moves along the streamlines created by the larger void, and that before the collision the shape and size of both voids are to a good approximation unchanging. The coalescence cross section σ is then

$$\sigma(\Omega_2, \Omega_1) = \pi \left(\frac{3}{4\pi} \right)^{2/3} \left[(\Omega_1^{1/3} + \Omega_2^{1/3})^2 - \frac{\Omega_1}{\Omega_1^{1/3} + \Omega_2^{1/3}} \right]. \quad (2)$$

This is smaller than the coalescence cross section for ballistic motion, $\pi(3/4\pi)^{2/3}[(\Omega_1^{1/3} + \Omega_2^{1/3})^2]$.

The rate with which voids of volume Ω coalesce with voids of volume Ω' is proportional to their velocity difference as well as their coalescence cross section. Let us denote this rate by $K(\Omega, \Omega')$, and write

$$K(\Omega, \Omega') = \sigma(\Omega_<, \Omega_>) \Delta v(\Omega_<, \Omega_>),$$

where the velocity difference is

$$\Delta v(\Omega_<, \Omega_>) \equiv v(\Omega_<) - v(\Omega_>) = k(\Omega_<^{-1/3} - \Omega_>^{-1/3}),$$

and where we have defined $\Omega_> \equiv \max(\Omega, \Omega')$ and $\Omega_< \equiv \min(\Omega, \Omega')$.

Now suppose that we have an infinitely long metal wire that occupies the region $0 \leq x < \infty$, $0 \leq y \leq L$, and $0 \leq z \leq L$. A specified number distribution of voids enters the wire at a constant rate on the plane $x=0$ and each void drifts in the x direction. Since voids of different radii travel at different speeds, voids collide and coalesce. Let $n(\Omega, x, t) d\Omega$ denote the average number of voids with volume between Ω and $\Omega + d\Omega$ per unit volume at a distance x away from the source. Our mean field equation of motion describes the evolution of $n(\Omega, x, t)$ by coalescence of pairs of voids of different sizes. It may be written as follows:

$$\begin{aligned} \frac{\partial n}{\partial t}(\Omega, x, t) + v(\Omega) \frac{\partial n}{\partial x}(\Omega, x, t) \\ = \frac{1}{2} \int_0^\Omega K(\Omega', \Omega - \Omega') n(\Omega', x, t) n(\Omega - \Omega', x, t) d\Omega' \\ - n(\Omega, x, t) \int_0^\infty K(\Omega, \Omega') n(\Omega', x, t) d\Omega'. \end{aligned} \quad (3)$$

The void distribution $n(\Omega, x, t)$ is affected by convective losses that occur at a rate which depends on the position x . This is accounted for by the second term on the left-hand side of Eq. (3). The first term on the right-hand side of Eq. (3) represents the increase in $n(\Omega, x, t)$ due to the coalescence of two voids of volume Ω' and $(\Omega - \Omega')$. The second term on the right-hand side of Eq. (3) represents the reduction in $n(\Omega, x, t)$ resulting from the collision of a void of volume Ω with another void.

A few comments on the form of Eq. (3) are in order. Note first that we have neglected the possibility that three or more voids simultaneously coalesce, and have taken only two void interactions into account. These approximations are reasonable when the void fraction in the wire is small. We also point out that when $n(\Omega, x, t)$ is independent of x , Eq. (3) reduces to the 3D analog of the mean field coagulation equation studied by Boularot and Bradley²² Finally, note that $K(\Omega, \Omega')$ is a homogeneous function of order 1/3, i.e., $K(a\Omega, a\Omega') = a^{1/3} K(\Omega, \Omega')$.

The number distribution is subject to the boundary condition $n(\Omega, 0, t) = n_0(\Omega)$, where $n_0(\Omega)$ is determined by the nature of the source. To completely specify the problem, the initial value $n(\Omega, x, 0)$ is needed for all Ω and $x \geq 0$. For simplicity, we will assume that $n(\Omega, x, 0) = 0$ for all Ω and x , so that initially the wire is entirely free of voids. In this case, the void size distribution for the entire system,

$$n(\Omega, t) \equiv \int_0^\infty \int_0^L \int_0^L n(\Omega, x, t) dx dy dz, \quad (4)$$

converges for all Ω and t .

III. DYNAMIC SCALING

In many coalescence processes, it is found that the cluster size distribution scales at long times.²⁸ We therefore expect that when t is large, the void size distribution $n(\Omega, t)$ will follow the scaling form

$$n(\Omega, t) = \Omega^{-\theta} g\left(\frac{\Omega}{t^z}\right), \quad (5)$$

where θ and z are dynamic critical exponents and g is the scaling function. We can go further and seek scaling solutions for the position-dependent void size distribution of the form

$$n(\Omega, x, t) = \Omega^{-\theta} h\left(\frac{\Omega}{x^\Delta}, \frac{\Omega}{t^z}\right).$$

If this scaling form is used in our problem, the critical exponent Δ turns out to be infinite—the present problem represents a singular limit of the general case.²⁹ Therefore, we will begin with the modified scaling ansatz

$$n(\Omega, x, t) = \Omega^{-\theta} f\left(\frac{\Omega}{e^{\rho x}}, \frac{\Omega}{t^z}\right), \quad (6)$$

where ρ is a positive constant that is to be determined. Inserting this into the equation of motion (3) and setting $\xi = \Omega/e^{\rho x}$, $\eta = \Omega/t^z$, and $\zeta = \Omega'/t^z$, we obtain

$$\begin{aligned} & \frac{1}{2} \int_0^\eta K(\zeta, \eta - \zeta) \zeta^{-\theta} (\eta - \zeta)^{-\theta} f\left(\frac{\xi}{\eta} \zeta, \zeta\right) f\left(\frac{\xi}{\eta} (\eta - \zeta), \eta - \zeta\right) d\zeta - \eta^{-\theta} f(\xi, \eta) \int_0^\infty K(\eta, \zeta) \zeta^{-\theta} f\left(\frac{\xi}{\eta} \zeta, \zeta\right) d\zeta \\ & = -\rho k t^{z(\theta-5/3)} \xi \eta^{-(\theta+1/3)} \frac{\partial}{\partial \xi} f(\xi, \eta) - z t^{z(\theta-4/3)-1} \eta^{1-\theta} \frac{\partial}{\partial \eta} f(\xi, \eta). \end{aligned} \tag{7}$$

Equation (7) shows that if a scaling solution of the form (6) exists, we must have

$$\theta = \frac{5}{3} \tag{8}$$

and

$$z = 3. \tag{9}$$

When these values for the dynamic critical exponents have been inserted into Eq. (7), we are left with a nonlinear integro-differential equation which could in principle be solved for the constant ρ and the scaling function f .

Let us explore the consequences of our results (8) and (9). Let Ω_0 be the mean volume of the voids injected at $x=0$. We will find it helpful to employ the dimensionless variables $\alpha \equiv \Omega/\Omega_0$ and $\tau \equiv t/t_0$, where $t_0 \equiv \Omega_0^{2/3}/k$. The scaling form (6) can then be written

$$n(\Omega, x, \tau) = \frac{1}{\Omega_0^2} \alpha^{-5/3} F\left(\frac{\alpha}{e^{\rho x}}, \frac{\alpha}{\tau^3}\right) \tag{10}$$

or, equivalently,

$$n(\Omega, x, \tau) = \frac{1}{\Omega_0^2} \tau^{-5} G\left(\frac{\alpha}{e^{\rho x}}, \frac{\alpha}{\tau^3}\right). \tag{11}$$

The scaling functions F and G are dimensionless and are easily related to f .

The total number of voids with volume between Ω and $\Omega + d\Omega$ at time t is $n(\Omega, t)d\Omega$, where $n(\Omega, t)$ is given by Eq. (4). Using the scaling form (11) and introducing the new variable of integration $u = e^{\rho x}/\alpha$, we obtain

$$n(\Omega, \tau) = \frac{L^2}{\rho \Omega_0^2 \tau^5} \int_{1/\alpha}^\infty G\left(\frac{1}{u}, \frac{\alpha}{\tau^3}\right) \frac{du}{u}. \tag{12}$$

When $\alpha = \Omega/\Omega_0 \gg 1$, we may set the lower limit of the integral in this expression to zero if $\int_0^\infty G(u^{-1}, \alpha/\tau^3) u^{-1} du$ is finite. We then have the scaling form

$$n(\Omega, \tau) = \tau^{-5} H\left(\frac{\Omega}{\tau^3}\right), \tag{13}$$

which is applicable for $\Omega \gg \Omega_0$.

The total volume occupied by the voids is $V(t) = \int_0^\infty n(\Omega, t) \Omega d\Omega$, which [using Eq. (12)] may be written

$$V(\tau) = \frac{L^2 \tau}{\rho} \Phi\left(\frac{1}{\tau}\right). \tag{14}$$

Here we have defined

$$\Phi(\zeta) \equiv \int_0^\infty \int_{\zeta^3/w}^\infty \frac{w}{u} G\left(\frac{1}{u}, w\right) dudw.$$

For $\tau \gg 1$, we have

$$V(\tau) \equiv \frac{\Phi(0)L^2}{\rho} \tau; \tag{15}$$

in other words, $V \propto \tau$ for large τ . This is certainly as it should be. Note, however, that with the boundary and initial conditions we have chosen, $V(\tau)/\tau$ is equal to a constant for all times, while it only tends to a constant as $\tau \rightarrow \infty$ in the scaling solution. As a result, the system only scales for sufficiently large times τ with our initial and boundary conditions.

For $\Omega \gg \Omega_0$, the number of voids per unit volume N is obtained from

$$N(\tau) \equiv \int_0^\infty n(\Omega, \tau) d\Omega = \int_0^\infty \tau^{-5} H\left(\frac{\Omega}{\tau^3}\right) \propto \tau^{-2}.$$

We then have the result that the average void volume $\langle \Omega \rangle \equiv V(\tau)/N(\tau) \propto \tau^3$ for $\tau \gg 1$ and $\Omega \gg \Omega_0$.

The void size distribution $n(\Omega, x, \tau)$ has a nontrivial dependence on the distance from the source which we will now study. Let $\phi(x, \tau) = \int_0^\infty n(\Omega, x, \tau) \Omega d\Omega$ be the void fraction at distance x from the source at time τ . Using Eq. (10) and introducing the new variable of integration $s = \alpha e^{-\rho x}$, we find that

$$\phi(x, \tau) = e^{\rho x/3} \Psi\left(\frac{\tau^3}{e^{\rho x}}\right), \tag{16}$$

where $\Psi(\zeta) \equiv \int_0^\infty F(s, s/\zeta) s^{-2/3} ds$.

Suppose that $\Psi(z) \sim Bz^\nu$ when z is large. (Here B and ν are constants.) We then have $\phi(x, \tau) \approx B\tau^{3\nu} \exp[(\frac{1}{3} - \nu)\rho x]$ for $\tau^3 \gg e^{\rho x}$. Now according to our boundary condition, $\phi(0, \tau) = \phi_0$, where $\phi_0 \equiv \int_0^\infty n_0(\Omega) \Omega d\Omega$. Therefore $\nu = 0$ and

$$\phi(x, \tau) \approx \phi_0 e^{\rho x/3} \tag{17}$$

for $\tau^3 \gg e^{\rho x}$. This means that for a fixed distance x from the origin, the void fraction tends to a steady state value $\phi_\infty(x)$ as $\tau \rightarrow \infty$, and, moreover, that $\phi_\infty(x)$ grows exponentially with x . Now consider the opposite limit in which $\tau^3 \ll e^{\rho x}$. We expect the scaling function $\Psi(z)$ to be analytic at the point $z=0$, and so we may perform a Taylor series expansion of it about this point. If this is so, then we have

$$\phi(x, \tau) = e^{\rho x/3} \left[\Psi(0) + \frac{\tau^3}{e^{\rho x}} \Psi'(0) + \dots \right], \tag{18}$$

where $\Psi'(z) \equiv d\Psi(z)/dz$. At any time τ , the void fraction will tend to zero as $x \rightarrow \infty$. Equation (18) then shows that we must have $\Psi(0) = 0$. We conclude that

$$\phi(x, \tau) \equiv \Psi'(0) \tau^3 e^{-2\rho x/3} \quad (19)$$

for $\tau^3 \ll e^{\rho x}$: i.e., the void fraction falls off exponentially with x when x is large. Equations (17) and (19), as well as the general scaling form (16), are in excellent agreement with the results of the simulations described in Sec. V.

Equations (17) and (19) show that, for a fixed value of τ , the void fraction grows exponentially with distance from the source, reaches a peak, and then decays exponentially with increasing distance. The larger, slower voids form a clot or traffic jam which captures most of the voids incident upon it. The clot drifts in the x direction, slowing down as it grows due to collisions with smaller voids. In fact, the position of the maximum of the void fraction is proportional to $\ln \tau$. To see this, let the position of the maximum of $\phi(x, \tau)$ at time τ be $x = x^*(\tau)$. Inserting Eq. (16) into the relation $\partial\phi(x^*, \tau)/\partial x = 0$, we find that

$$\Psi(\tau^3 e^{-\rho x^*}) = 3\tau^3 e^{-\rho x^*} \Psi'(\tau^3 e^{-\rho x^*}).$$

Thus, $\tau^3 e^{-\rho x^*} = \omega_0$, where ω_0 is a dimensionless constant. We conclude that

$$x^*(\tau) \sim \frac{3}{\rho} \ln \tau \quad (20)$$

for $\tau \gg 1$.

Finally, we note that the analysis of this section is easily extended to the two-dimensional case in which the voids are circular. In two dimensions, we find $\theta = 3/2$ and $z = 3$. The number distribution for voids of area a obeys the scaling form

$$n(a, \tau) = \tau^{-3} H_2\left(\frac{a}{\tau^2}\right),$$

while the void fraction satisfies

$$\phi(x, \tau) = e^{\rho x/2} \Psi_2\left(\frac{\tau^2}{e^{\rho x}}\right),$$

where H_2 and Ψ_2 are scaling functions. The two-dimensional analogs to Eqs. (17) and (19) are then

$$\phi(x, \tau) \equiv \phi_0 e^{\rho x/2} \quad \text{for } \tau^2 \gg e^{\rho x},$$

and

$$\phi(x, \tau) \equiv \Psi'(0) \tau^2 e^{-\rho x/2} \quad \text{for } \tau^2 \ll e^{\rho x}.$$

The average area of the voids increases linearly in time,²² in contrast to the 3D result $\langle \Omega \rangle \propto \tau^3$. As in three dimensions, the total area occupied by the voids grows linearly in time. These predictions agree well with simulations.³⁰

IV. STEADY STATE SCALING SOLUTIONS

We now consider the steady state properties of our model. At long times, the volume distribution $n(\Omega, x, \tau)$ should become independent of time for a given value of x . To study the time-independent properties, we set $\partial n/\partial t = 0$ in Eq. (3)

and make the following definitions:

$$\tilde{K}(\Omega, \Omega') \equiv \frac{K(\Omega, \Omega')}{v(\Omega)v(\Omega')}$$

and

$$\tilde{n}(\Omega, x) \equiv v(\Omega)n(\Omega, x).$$

Note that the new kernel \tilde{K} is homogeneous with homogeneity index $\lambda = 1$. The equation of motion becomes

$$\begin{aligned} \frac{\partial \tilde{n}}{\partial x}(\Omega, x) = & \frac{1}{2} \int_0^\Omega \tilde{K}(\Omega', \Omega - \Omega') \tilde{n}(\Omega', x) \tilde{n}(\Omega - \Omega', x) d\Omega' \\ & - \tilde{n}(\Omega, x) \int_0^\infty \tilde{K}(\Omega, \Omega') \tilde{n}(\Omega', x) d\Omega'. \end{aligned} \quad (21)$$

If we make the formal replacement $x \rightarrow t$, Eq. (21) becomes the coagulation equation of Schmolukowski with kernel \tilde{K} .³¹ As we have noted in Sec. I, there have been many studies of the scaling properties of Eq. (21) with particular choices of the kernel. van Dongen and Ernst provide the most complete accounting of the scaling properties of Eq. (21).³² They obtain scaling solutions classified by the homogeneity index λ and the large argument behavior of the kernel. However, their analysis is valid only for $\lambda \neq 1$. We now carry out an analysis for our problem (in which $\lambda = 1$) to obtain approximate scaling solutions to Eq. (21).

We begin by constructing a scaling form for $\tilde{n}(\Omega, x)$. Let $n(\Omega, x) \equiv \lim_{\tau \rightarrow \infty} n(\Omega, x, \tau)$. From Eq. (10) we see that $n(\Omega, x) = \Omega^{-5/3} F_0(\Omega/e^{\rho x})$ where $F_0(\xi) \equiv \Omega_0^{-1/3} F(\xi, 0)$. We then have $\tilde{n}(\Omega, x) = k \Omega^{-2} F_0(\Omega/e^{\rho x})$ or, equivalently,

$$\tilde{n}(\Omega, x) = e^{-2\rho x} \tilde{H}\left(\frac{\Omega}{e^{\rho x}}\right). \quad (22)$$

Our goal is to determine the form of $\tilde{H}(z)$ as $z \rightarrow \infty$. Consider the quantity $J(\Omega, x, t)$ defined by

$$J(\Omega, x, t) \equiv \int_0^\Omega \Omega' v(\Omega') n(\Omega', x, t) d\Omega'. \quad (23)$$

$J(\Omega, x, t)$ is the integrated flux of voids with volumes less than or equal to Ω at position x in the wire and at time t . The total void flux $J(x, t) \equiv \lim_{\Omega \rightarrow \infty} J(\Omega, x, t)$ must satisfy the continuity equation

$$\frac{\partial J(x, t)}{\partial x} + \frac{\partial \phi(x, t)}{\partial t} = 0.$$

In the steady state regime, $\partial \phi(x, t)/\partial t = 0$, so that $J(x, t)$ approaches a constant independent of x for $t \rightarrow \infty$. Call this constant J_0 . We define the steady state analog to $J(\Omega, x, t)$ as

$$J_s(\Omega, x) \equiv \lim_{t \rightarrow \infty} J(\Omega, x, t) = \int_0^\Omega \Omega' \tilde{n}(\Omega', x) d\Omega'. \quad (24)$$

We then have the result that $J_s(\Omega, x)$ approaches J_0 as $\Omega \rightarrow \infty$. Computing the divergence of $J_s(\Omega, x)$ results in

$$-\frac{\partial J_s(\Omega, x)}{\partial x} = 2\rho e^{-2\rho x} \int_0^\Omega \tilde{H}'\left(\frac{\Omega'}{e^{\rho x}}\right) d\Omega' + \rho e^{-3\rho x} \int_0^\Omega (\Omega')^2 \tilde{H}'\left(\frac{\Omega'}{e^{\rho x}}\right) d\Omega', \quad (25)$$

where $\tilde{H}'(z) \equiv d\tilde{H}/dz$. We differentiate Eq. (25) with respect to Ω and obtain

$$-\frac{\partial}{\partial x} \frac{\partial J_s}{\partial \Omega}(\Omega, x) = 2\rho e^{-2\rho x} \Omega \tilde{H}'\left(\frac{\Omega}{e^{\rho x}}\right) + \rho e^{-3\rho x} \Omega^2 \tilde{H}'\left(\frac{\Omega}{e^{\rho x}}\right). \quad (26)$$

As $\Omega \rightarrow \infty$, the left side of Eq. (26) tends to zero since $\partial J_s / \partial \Omega \rightarrow 0$ as $\Omega \rightarrow \infty$. We then have the differential equation

$$z \frac{d\tilde{H}(z)}{dz} + 2\tilde{H}(z) \equiv 0, \quad (27)$$

which is valid for large $z \equiv \Omega e^{-\rho x}$. Equation (27) has the solution

$$\tilde{H}(z) \equiv \frac{c}{z^2} \quad \text{for } z \gg 1, \quad (28)$$

where c is a constant.

Finally, we obtain the desired large Ω steady state scaling forms of the void volume distribution:

$$\tilde{n}(\Omega, x) = e^{-2\rho x} \tilde{H}\left(\frac{\Omega}{e^{\rho x}}\right) \sim \Omega^{-2}$$

and

$$n(\Omega, x) \sim \Omega^{-5/3}, \quad (29)$$

which are applicable when $\Omega \gg e^{\rho x}$.

Equation (28) implies that the scaling function H [Eq. (13)] also behaves as a power law in the scaling regime ($\tau \gg 1$) when $\Omega \gg \tau^3$. To be explicit,

$$H(\zeta) \sim \zeta^{-5/3} \quad \text{for } \zeta \gg 1. \quad (30)$$

This leads to the result that $n(\Omega, \tau)$ is independent of τ for $\Omega \gg \tau^3$ in the scaling regime.

V. MONTE CARLO SIMULATIONS

We begin by briefly describing the algorithm used to study the coalescence kinetics. Consider a long wire with a square cross section of area $A \equiv L^2$, i.e., $L_y = L_z = L$. We choose the units of distance so that $L = 1$, and the long dimension of the wire L_x is chosen to be 200. The natural time scale is set by $t_0 \equiv \Omega_0^{2/3}/k$. We choose the units of time so that $t_0 = 1$. At $t = 0$ a small number of voids are introduced with their centers at random positions on the plane $x = 0$ (the anode). As the number of voids per injection step is quite small, overlaps at $x = 0$ are exceedingly rare. If the random placement does result in an overlap, all of the injected voids are removed from the $x = 0$ plane, and new random positions are obtained and used for placement. We will restrict our attention to the case in which the void fraction is small, so that the simultaneous interaction between more than two

voids is a rare event. By choosing a sufficiently low rate of void injection and requiring that $\Omega_0 \ll 1$, the void fraction in the wire is kept small.

We choose the initial distribution function to be $n_0(\Omega) = \exp(-\Omega/200)$, so that the mean void volume at $x = 0$ is $\Omega_0 = 5 \times 10^{-3}$. While this is a convenient choice of $n_0(\Omega)$, the long-time properties of the model are independent of the particular form of $n_0(\Omega)$. More pathological forms of $n_0(\Omega)$ result in longer computation time before the scaling regime is reached. With $\Omega_0 = 5 \times 10^{-3}$, the total void fraction never exceeds 10^{-3} and the local void fraction never exceeds 10^{-2} in any region of the wire.

Having obtained an initial distribution of voids, the voids are advanced ballistically for a time δt_I which we define as the time between injections and which is chosen to be $\delta t_I = 10t_0 = 10$. The injection process is repeated, and now the potential for collisions arises. We adopt the rule that two voids coalesce only if their impact parameter is smaller than $[\sigma(\Omega', \Omega)/\pi]^{1/2}$. In this way, the effects of current crowding are taken into account in an approximate fashion. A list of voids sorted by their x coordinates is used to construct, for each void i , a small subset of voids j for which a collision may occur before the next injection. For each pair of voids (i, j) , the time to their coalescence is computed, assuming no other collisions occur involving either void i or void j . Let this time interval for void pairs (i, j) be t_c^{ij} . All collision times $t_c^{ij} < t_I$ (if any) are obtained, and the voids are advanced through a time $t_{\min} \equiv \min(t_c^{ij})$, whereupon the colliding voids of volume Ω_i and Ω_j are coalesced to obtain a new void of volume $\Omega_i + \Omega_j$. The coordinates of the new void are prescribed by the condition that the collision not alter the center of mass of the two voids. Collision times are again obtained and the voids are advanced to the next coalescence. This process is repeated until the next injection time is reached. An injection then occurs, beginning a new iteration of the algorithm. In practice, the void fraction is small enough that there are typically zero, one, or two collisions between each injection step. Voids whose centers have reached the plane $x = L_x$ are discarded from the simulation volume.

The algorithm is iterated through 5000 coalescence events. At regular intervals of τ , the number and volume distributions are calculated and used to construct $\phi(x, \tau)$ and $n(\Omega, \tau)$. We then average the distributions of 30 000 such simulations to obtain the results described below.

In Fig. 1, $n(\Omega, \tau)$ is plotted against Ω for 30 equally spaced values of τ in the interval $400 \leq \tau \leq 6000$. Note that the transition from the initial distribution $n_0(\Omega)$ to a steady state form is evident as τ increases. The small- τ curves do not differ significantly from the exponential distribution present at $\tau = 0$, while the large- τ behavior approaches a form independent of τ . The dashed curve corresponds to the distribution at $\tau = 400$, where the data still follows the form of the initial distribution closely.

According to Eqs. (13) and (30), $\tau^5 n(\Omega, \tau)$ should scale as a power law in the variable Ω/τ^3 for $\Omega \gg \Omega_0$ and $\Omega \gg \tau^3$ in the scaling regime $\tau \gg 1$. This power law scaling is confirmed in Fig. 2. The slope of the log-log plot in Fig. 2 is 1.67 ± 0.01 , in agreement with the prediction of the steady state scaling analysis of Sec. IV, where we found $H(\zeta) \sim \zeta^{-5/3}$. The data in Fig. 2 span the same range in τ as

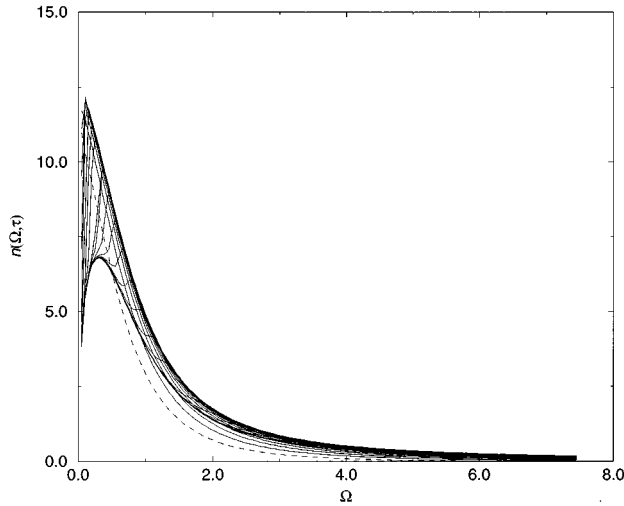


FIG. 1. $n(\Omega, \tau)$ vs Ω is shown for 30 equally spaced values of τ in the range $400 \leq \tau \leq 6000$. The dashed curve corresponds to the distribution at $\tau = 400$ and shows the exponential character of the initial distribution $n_0(\Omega)$. The units on both axes are arbitrary.

that in Fig. 1. The breakdown in scaling for very large Ω/τ^3 occurs in the short-time regime, where the initial distribution $n_0(\Omega)$ dominates $n(\Omega, \tau)$.

We now examine the scaling properties of the void fraction $\phi(x, \tau)$. The essential predictions are contained in Eqs. (16), (17), and (19). Figure 3 shows $\ln \phi(x, \tau)$ vs x for τ in the interval $5.0 \times 10^3 \leq \tau \leq 1.5 \times 10^4$. As predicted by the scaling theory, the void fraction increases exponentially with x , reaches a maximum, and then decreases monotonically. For $\tau^3 \gg e^{\rho x}$, $\phi(x, \tau)$ is clearly independent of τ , and is exponential in x . For $\tau^3 \ll e^{\rho x}$, $\phi(x, \tau)$ is again exponential in x , but also displays some time dependence. Computing the slopes of $\ln \phi(x, \tau)$ in both scaling regimes, we find $\rho = 0.054 \pm 0.002$. A scaling plot of $\phi(x, \tau)/\tau^3$ vs x shows

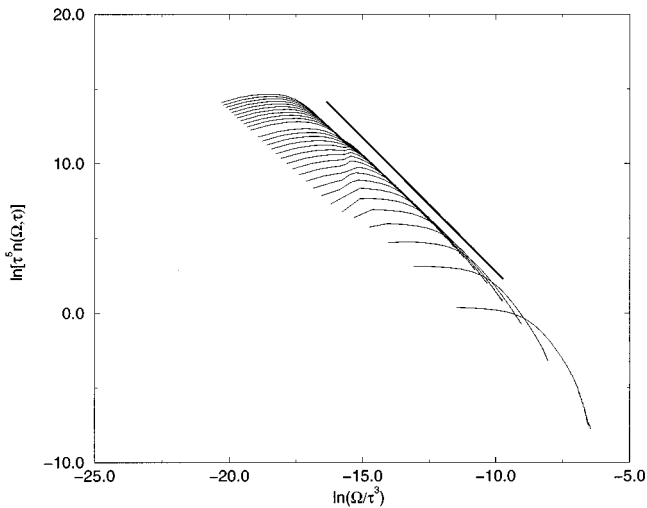


FIG. 2. $\tau^5 n(\Omega, \tau)$ vs Ω/τ^3 is shown in a log-log plot for 30 equally spaced values of τ in the range $400 \leq \tau \leq 6000$. The thick line has slope $-5/3$. The units on both axes are arbitrary. The logarithms are base e .

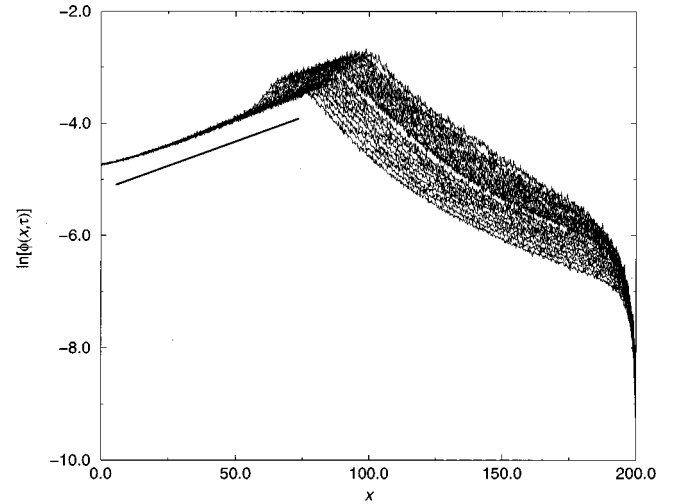


FIG. 3. $\ln[\phi(x, \tau)]$ is plotted against x for 20 values of τ in the range $5.0 \times 10^3 \leq \tau \leq 1.5 \times 10^4$. The thick line has slope 0.018.

good collapse of the data onto the scaling form (19) for $e^{\rho x} \gg \tau^3$ (Fig. 4). Measuring the slope of the curves, we again find $\rho \approx 0.054$.

It is also useful to examine the validity of the general scaling form, Eq. (16). In Fig. 5 $\phi(x, \tau)/e^{\rho x/3}$ is plotted against $\tau^3/e^{\rho x}$ for ten equally spaced values of τ spanning the range $7.0 \times 10^3 \leq \tau \leq 1.5 \times 10^4$. For $\rho = 0.054$, we find excellent collapse of the data. The $\tau^3 \gg e^{\rho x}$ scaling regime is marked by the zero-slope region of the curves in Fig. 5. By Eq. (17), $\phi(x, \tau)/e^{\rho x/3}$ tends to the constant ϕ_0 in this regime. In the opposite limit, $\tau^3 \ll e^{\rho x}$, we find that $\phi(x, \tau)e^{-\rho x/3} \propto \tau^3/e^{\rho x}$, in agreement with Eq. (19). The solid line in Fig. 5 has slope 1.0.

VI. SUMMARY

Electromigration failure of metal interconnects is preceded by the formation, drift, and coalescence of a collection

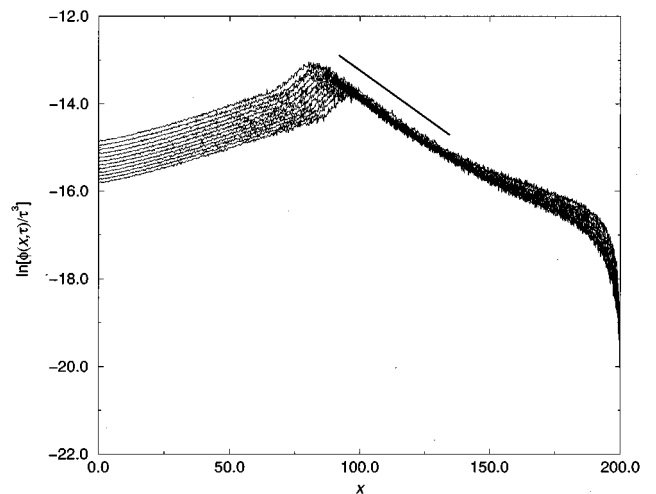


FIG. 4. $\ln[\phi(x, \tau)\tau^{-3}]$ vs x is shown for 20 values of τ in the range $5.0 \times 10^3 \leq \tau \leq 1.5 \times 10^4$. The breakdown of scaling near $x = 150$ is a finite-size effect. The thick line has slope -0.036 .

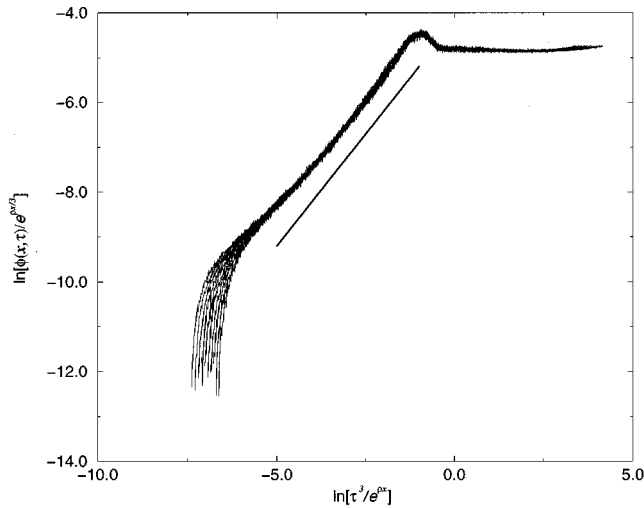


FIG. 5. A scaling plot of $\phi(x, \tau)e^{-\rho x/3}$ vs $\tau^3 e^{-\rho x}$ shows collapse of the data onto the scaling function Ψ for $\rho=0.054$. The thick line has slope 1.0. The units on both axes are arbitrary.

of voids. That the dynamics of this collection bear directly on the lifetime of the interconnect has been experimentally verified by many workers.^{9,33} To date, however, there has been relatively little attention directed toward understanding the dynamics of such a collection.

In this paper, we have proposed an approximate mean field theory for the drift and coalescence of spherical voids in a single-crystal metal line. Our mean field equation takes explicit account of the spatial inhomogeneity of the void distributions arising from the presence of a source of voids. In the absence of a source of voids, our Eq. (3) reduces to a special case of the much studied coagulation equation²⁸ for which scaling solutions exist for a variety of coagulation kernels.^{32,34} The scaling properties of Eq. (3), however, are markedly different. While the void distribution $n(\Omega, x, t)$ scales in both time and space, the spatial scaling is described by the marginal scaling variable $\Omega e^{-\rho x}$. Specifically,

$$n(\Omega, x, t) = \Omega^{-\theta} f\left(\frac{\Omega}{e^{\rho x}}, \frac{\Omega}{t^z}\right),$$

where the mean field values of θ and z were found to be $\theta=5/3$ and $z=3$ in 3D. These values are in good agreement with the results of the Monte Carlo simulations described in Sec. V. The value of ρ obtained in the simulations is $\rho=0.054 \pm 0.002$.

The integrated void volume distribution $n(\Omega, \tau)$ was shown to obey the scaling form

$$n(\Omega, \tau) = \tau^{-5} H\left(\frac{\Omega}{\tau^3}\right),$$

which is applicable for $\Omega \gg \Omega_0$. When $\Omega \gg \tau^3$, the scaling function $H(z)$ behaves as $H(z) \propto z^{-5/3}$, so that $n(\Omega, \tau) \propto \Omega^{-5/3}$ for large Ω/τ^3 .

The void fraction $\phi(x, \tau)$ is given by

$$\phi(x, \tau) = e^{\rho x/3} \Psi\left(\frac{\tau^3}{e^{\rho x}}\right).$$

Approximate expressions for $\phi(x, \tau)$ were obtained in the two scaling limits $e^{\rho x} \ll \tau^3$ and $e^{\rho x} \gg \tau^3$. When $\tau^3 \gg e^{\rho x}$, we find $\phi(x, \tau) \cong \phi_0 e^{\rho x/3}$. In the opposite limit, $\tau^3 \ll e^{\rho x}$, we have $\phi(x, \tau) \cong \Psi'(0) \tau^3 e^{-2\rho x/3}$. In both scaling regimes, the predictions of the scaling theory are in excellent agreement with the results of the simulations. At a fixed value of τ , the void fraction increases monotonically with x , reaching a peak where large, slow moving voids have formed. The void flux downstream of this obstruction is reduced and $\phi(x, \tau)$ decreases monotonically with x beyond the position of the largest void. The position of the maximum of $\phi(x, \tau)$ increases as $\ln \tau$.

It is worth emphasizing that our theory describes the *initial* stages of failure due to electromigration in metallic interconnects. Early in the time evolution of the conductor, the voids are small compared to the interconnect dimensions and have a spherical form. In the later stages of the interconnect's failure, the voids are no longer spherical; their growth is impeded by the surfaces of the interconnect. Our theory does not describe the void dynamics in the later stages of failure and therefore does not provide lifetime estimates. The time evolution of the void size distribution in the early stages of failure is, however, experimentally accessible. Transmission electron microscopy could be used to image migrating voids in free-standing, current-carrying thick films, just as it is used to observe submicrometer-sized helium bubbles in metal films that have been irradiated with α particles.^{35,36} While there have been preliminary investigations of EM-induced void dynamics in near-bamboo thin films,⁹ there is a real need for experimental work on bulk, single-crystal samples in which the effects of the boundaries and of crystalline disorder can be neglected. We hope that our work will stimulate more quantitative experimental work on void dynamics in samples of this kind.

ACKNOWLEDGMENTS

We would like to thank S. Redner and M. Mahadevan for useful discussions. This work was supported in part by NSF Grant No. DMR-9100257.

¹H. B. Huntington, in *Diffusion in Solids—Recent Developments*, edited by A. S. Novick and J. J. Burton (Academic, New York, 1975).

²J. N. Pratt and R. G. R. Sellors, *Electrotransport in Metals and Alloys* (Trans Tech, Riechen, 1973).

³D. A. Rigney, in *Charge Transfer—Electronic Structure of Al-*

loys, edited by L. H. Bennett and R. H. Willens (AIME, New York, 1974).

⁴F. M. d'Heurle and P. S. Ho, in *Thin Films—Interdiffusion and Reactions*, edited by J. M. Poate, K. N. Tu, and J. W. Mayer (John Wiley, New York, 1978).

⁵P. B. Ghatge, *Solid State Technol.* **26**, 113 (1983).

- ⁶P. S. Ho, J. Appl. Phys. **41**, 64 (1970).
- ⁷M. Mahadevan and R. M. Bradley, J. Appl. Phys. **79**, 6840 (1996).
- ⁸W. Wang, Z. Suo, and T.-H. Hao, J. Appl. Phys. **79**, 2394 (1996).
- ⁹K. Hinode, S. Kondo, and O. Deguchi, J. Vac. Sci. Technol. B **14**, 687 (1996).
- ¹⁰M. J. Attardo, R. Rutledge, and R. C. Jack, J. Appl. Phys. **42**, 4343 (1971).
- ¹¹J. M. Schoen, J. Appl. Phys. **51**, 513 (1980).
- ¹²H. B. Huntington, A. Kalukin, P. P. Meng, Y. T. Shy, and S. Ahmad, J. Appl. Phys. **70**, 1359 (1991).
- ¹³P. J. Marcoux, P. P. Merchant, V. Naroditsky, and W. D. Rehder, Hewlett-Packard J. **40**, 79 (1989).
- ¹⁴R. Kirchheim and U. Kaeber, J. Appl. Phys. **70**, 172 (1991).
- ¹⁵T. J. Smy, S. S. Winterton, and M. J. Brett, J. Appl. Phys. **73**, 2821 (1993).
- ¹⁶J. T. Trattles, A. G. O'Neill, and B. C. Mecrow, J. Appl. Phys. **75**, 7799 (1994).
- ¹⁷R. M. Bradley and K. Wu, J. Phys. A **27**, 327 (1994).
- ¹⁸R. M. Bradley and K. Wu, Phys. Rev. E **50**, R631 (1994).
- ¹⁹K. Wu and R. M. Bradley, Phys. Rev. B **50**, 12 468 (1994).
- ²⁰S. Vaidya, T. T. Sheng, and A. K. Sinha, Appl. Phys. Lett. **36**, 464 (1980).
- ²¹L. K. Wickham and J. P. Sethna, Phys. Rev. B **51**, 15 017 (1995).
- ²²H. Boularot and R. M. Bradley, J. Appl. Phys. **80**, 756 (1996).
- ²³D. Chae and P. B. Dubovskii, Z. Angew. Math. Phys. **46**, 580 (1995).
- ²⁴P. B. Dubovskii, Differential Equations **26**, 380 (1990).
- ²⁵Z. Cheng, S. Redner, and F. Leyvraz, Phys. Rev. Lett. **62**, 2321 (1989).
- ²⁶P. Meakin, Phys. Rev. A **40**, 2655 (1989).
- ²⁷P. Meakin, Phys. Rev. A **42**, 4678 (1990).
- ²⁸T. Vicsek, *Fractal Growth Phenomena* (World Scientific, Singapore, 1989).
- ²⁹R. M. Bradley (unpublished).
- ³⁰H. Boularot and R. M. Bradley (unpublished).
- ³¹See, for example, S. K. Friedlander, *Smoke, Dust and Haze* (Wiley, New York, 1977).
- ³²P. G. J. van Dongen and M. H. Ernst, Phys. Rev. Lett. **54**, 1396 (1985).
- ³³S. Shingubara, H. Kaneko, and M. Saitoh, J. Appl. Phys. **69**, 207 (1991), and references therein.
- ³⁴P. G. J. van Dongen and M. H. Ernst, J. Phys. A **18**, 2779 (1985).
- ³⁵R. S. Barnes and D. J. Mazey, Proc R. Soc. London, Sect. A **275**, 47 (1963).
- ³⁶F. A. Nichols, J. Nucl. Mater. **30**, 143 (1969).